*Progress In Electromagnetics Research*, PIER 99, 21–36, 2009

# ANALYSIS OF SCATTERING BY LARGE INHOMOGENEOUS BI-ANISOTROPIC OBJECTS USING AIM

**L. Hu, L.-W. Li, and T.-S. Yeo**

Department of Electrical and Computer Engineering
National University of Singapore
Singapore 119260, Singapore

**Abstract**—In this paper, electromagnetic scattering of a plane wave by large inhomogeneous arbitrarily shaped bi-anisotropic objects is solved by Adaptive Integral Method (AIM). Based on Maxwell equations and constitutive relationship for general bi-anisotropic media and using Volume Integral Equations (VIE), the electromagnetic fields are derived as functions of equivalent volume sources. Then the integral equations are discretized using Method of Moments (MoM). Because of the dense matrix property, MoM cannot be used to solve electromagnetic scattering by large objects. Therefore, AIM is adopted to reduce the memory requirement and speed up the solution process. Comparison between AIM and MoM with respect to CPU time and memory requirement is done to show the efficiency of AIM in solving electromagnetic scattering by large objects. Numerical results are obtained for some canonical cases and compared with Mie theory, in which excellent agreement is observed. some new numerical results are also presented for the more general bi-anisotropic material media.

## 1. INTRODUCTION

There has been a growing interest recently in the study of interaction between electromagnetic fields and bi-anisotropic materials [1]. Bi-anisotropic media incorporates large variety of media, such as chiral or bi-isotropic media, gyrotropic chiral media, Faraday chiral media, anisotropic media, and gyrotropic media. Various applications utilizing bi-anisotropic media have been proposed such as angle-sensitive beam-shaping cover for antennas [2], negative refractive index [3–5], giant negative Goos-Hänchen shifter [6], polarization transformer [7], electromagnetic transparent coatings and shielding [8, 9], scattering enhancement by radial anisotropy [10, 11], and RF circuits [12].

Corresponding author: L. Hu (huli@nus.edu.sg).

Electromagnetic scattering is one of the basic problems in the study of interaction between electromagnetic waves and bi-anisotropic objects. A rigorous solution of scattered fields by spheres can be obtained using Mie theory [13–15]. However, if the structures of complex media are not in canonical geometries, the analytical analysis is limited and not capable then. In this connection, many numerical methods have been extended to study the interaction of electromagnetic wave with complex media such as FDTD [16], FEM [17] and FEM-BEM [18].

MoM has also been used to solve arbitrary three dimensional problems with more general types of materials. Scattering by arbitrarily shaped inhomogeneous dielectric bodies was solved in [19]. Scattering by a gyroelectric body with arbitrary inhomogeneity was tackled in [20]. The scattering problem of inhomogeneous chiral objects was studied in [21]. When using MoM to solve electromagnetic scattering problems by bi-anisotropic objects, the direct solver requires $O(N^3)$ operations to solve such linear equations with N number of unknowns, while the iterative solver requires $O(N_{iter}N^2)$ operations where $N_{iter}$ is the number of iterations. Both methods require $O(N^2)$ memory to store the dense matrix. Thus, the stringent computational and memory requirements have impeded MoM from solving large scale problems which prevails in real life. However, the recently developed fast solvers such as AIM and p-FFT [22–26] can alleviate the difficulties above. The attracting feature of it is the computational and memory requirement are respectively $O(N \log N)$ and $O(N)$ based on volume integral equations.

In this paper, the electromagnetic scattering by large arbitrarily shaped inhomogeneous bi-anisotropic objects is solved by AIM. Volume integral equation approach is presented and free-space Green's function is used in the formulation of integral equations. Based on Maxwell equations and constitutive relationship for general bi-anisotropic media, electromangetic fields are expressed as functions of equivalent volume electric and magnetic currents. Then MoM is used to convert the resultant equation into matrix equations which are subsequently solved by using an iterative solver. AIM is used to accelerate the solution process and to reduce the memory requirement for matrix storage. Some canonical cases are considered and the results are calculated using AIM and compared with Mie theory. Excellent agreement is observed. After the validation of the numerical solver, some new results are computed and discussed.

## 2. FORMULATION

### 2.1. Volume Integral Equations

Consider a homogeneous background medium with permittivity $\epsilon_0$ and permeability $\mu_0$. If an inhomogeneous bi-anisotropic body is present in the background, the fields in the region of bi-anisotropic body must satisfy Maxwell equation:

$$\nabla \times \mathbf{E} = -j\omega \mathbf{B} = -j\omega\mu_0 \mathbf{H} - \mathbf{M}_V \tag{1}$$
$$\nabla \times \mathbf{H} = j\omega \mathbf{D} = j\omega\epsilon_0 \mathbf{E} + \mathbf{J}_V \tag{2}$$

The constitutive relations for bi-anisotropic media are:

$$\mathbf{D} = \bar{\boldsymbol{\epsilon}} \cdot \mathbf{E} + \bar{\boldsymbol{\xi}} \cdot \mathbf{H} \tag{3}$$
$$\mathbf{B} = \bar{\boldsymbol{\zeta}} \cdot \mathbf{E} + \bar{\boldsymbol{\mu}} \cdot \mathbf{H} \tag{4}$$

which can be written as:

$$\mathbf{E} = \bar{\boldsymbol{\alpha}}_1 \cdot \mathbf{D} + \bar{\boldsymbol{\alpha}}_2 \cdot \mathbf{B} \tag{5}$$
$$\mathbf{H} = \bar{\boldsymbol{\alpha}}_3 \cdot \mathbf{D} + \bar{\boldsymbol{\alpha}}_4 \cdot \mathbf{B} \tag{6}$$

where the parameters are:

$$\begin{bmatrix} \bar{\boldsymbol{\alpha}}_1 & \bar{\boldsymbol{\alpha}}_2 \\ \bar{\boldsymbol{\alpha}}_3 & \bar{\boldsymbol{\alpha}}_4 \end{bmatrix} = \begin{bmatrix} \bar{\boldsymbol{\epsilon}} & \bar{\boldsymbol{\xi}} \\ \bar{\boldsymbol{\zeta}} & \bar{\boldsymbol{\mu}} \end{bmatrix}^{-1} \tag{7}$$

The expression of equivalent volume sources are:

$$\mathbf{J}_V = j\omega(\bar{\boldsymbol{\epsilon}} - \epsilon_0 \bar{\mathbf{I}}) \cdot \mathbf{E} + j\omega \bar{\boldsymbol{\xi}} \cdot \mathbf{H} \tag{8}$$
$$\mathbf{M}_V = j\omega(\bar{\boldsymbol{\mu}} - \mu_0 \bar{\mathbf{I}}) \cdot \mathbf{H} + j\omega \bar{\boldsymbol{\zeta}} \cdot \mathbf{E} \tag{9}$$

which can be written as:

$$\mathbf{J}_V = j\omega(\bar{\boldsymbol{\beta}}_1 \cdot \mathbf{D} + \bar{\boldsymbol{\beta}}_2 \cdot \mathbf{B}) \tag{10}$$
$$\mathbf{M}_V = j\omega(\bar{\boldsymbol{\beta}}_3 \cdot \mathbf{D} + \bar{\boldsymbol{\beta}}_4 \cdot \mathbf{B}) \tag{11}$$

where the parameters are defined as:

$$\begin{bmatrix} \bar{\boldsymbol{\beta}}_1 & \bar{\boldsymbol{\beta}}_2 \\ \bar{\boldsymbol{\beta}}_3 & \bar{\boldsymbol{\beta}}_4 \end{bmatrix} = \begin{bmatrix} \bar{\mathbf{I}} - \epsilon_0 \bar{\boldsymbol{\alpha}}_1 & -\epsilon_0 \bar{\boldsymbol{\alpha}}_2 \\ -\mu_0 \bar{\boldsymbol{\alpha}}_3 & \bar{\mathbf{I}} - \mu_0 \bar{\boldsymbol{\alpha}}_4 \end{bmatrix} \tag{12}$$

Using mixed potential expression for source field relationship, the scattering fields can be expressed by:

$$\mathbf{E}^{\text{sca}} = -j\omega \mathbf{A} - \nabla \phi_e - \nabla \times \frac{\mathbf{F}}{\epsilon_0} \tag{13}$$
$$\mathbf{H}^{\text{sca}} = -j\omega \mathbf{F} - \nabla \phi_m + \nabla \times \frac{\mathbf{A}}{\mu_0} \tag{14}$$

where $\mathbf{A}, \mathbf{F}, \phi_e, \phi_m$ are magnetic vector potential, electric vector potential, electric scalar potential, magnetic scalar potential which can be expressed by:

$$\mathbf{A} = \mu_0 \int_V \mathbf{J}_V G dV' \tag{15}$$

$$\mathbf{F} = \epsilon_0 \int_V \mathbf{M}_V G dV' \tag{16}$$

$$\phi_e = \frac{1}{\epsilon_0} \int_V \rho_e G dV' \tag{17}$$

$$\phi_m = \frac{1}{\mu_0} \int_V \rho_m G dV' \tag{18}$$

where $G$ is the free space Green's function:

$$G(\mathbf{r}, \mathbf{r}') = \frac{e^{-jk_0|\mathbf{r}-\mathbf{r}'|}}{4\pi|\mathbf{r}-\mathbf{r}'|} \tag{19}$$

The relations between equivalent volume charge densities and currents are:

$$\rho_e = -\frac{1}{j\omega} \nabla \cdot \mathbf{J}_V \tag{20}$$

$$\rho_m = -\frac{1}{j\omega} \nabla \cdot \mathbf{M}_V \tag{21}$$

Since the total fields are the sum of incident fields and scattering fields induced by the bi-anisotropic body:

$$\mathbf{E} = \mathbf{E}^{\text{inc}} + \mathbf{E}^{\text{sca}} \tag{22}$$

$$\mathbf{H} = \mathbf{H}^{\text{inc}} + \mathbf{H}^{\text{sca}} \tag{23}$$

based on Eqs. (5), (6) and Eqs. (13), (14), we obtain volume electric and magnetic integral equations:

$$\mathbf{E}^{\text{inc}} = \bar{\boldsymbol{\alpha}}_1 \cdot \mathbf{D} + \bar{\boldsymbol{\alpha}}_2 \cdot \mathbf{B} + j\omega\mathbf{A} + \nabla\phi_e + \nabla \times \frac{\mathbf{F}}{\epsilon_0} \tag{24}$$

$$\mathbf{H}^{\text{inc}} = \bar{\boldsymbol{\alpha}}_3 \cdot \mathbf{D} + \bar{\boldsymbol{\alpha}}_4 \cdot \mathbf{B} + j\omega\mathbf{F} + \nabla\phi_m - \nabla \times \frac{\mathbf{A}}{\mu_0} \tag{25}$$

## 2.2. Method of Moments

The inhomogeneous bi-anisotropic objects are divided into tetrahedrons and for each face of the tetrahedron, we assign a basis function.

For the easy implementation, we employ the famous SWG basis function [19] which is defined below:

$$\mathbf{f}_n(\mathbf{r}) = \begin{cases} \dfrac{A_n}{3V_n^+}\rho_n^+, & \mathbf{r} \in T_n^+ \\ \dfrac{A_n}{3V_n^-}\rho_n^-, & \mathbf{r} \in T_n^- \end{cases} \tag{26}$$

where $A_n$ is the area of the $n$th face, $T_n^\pm$ is the the plus/minus tetrahedron of the $n$th face and $V_n^\pm$ are their volumes, $\rho_n^\pm$ is the position vector with respect to the free vertex of $T_n^\pm$. The gradient of SWG basis function is:

$$\nabla \cdot \mathbf{f}_n(\mathbf{r}) = \begin{cases} \dfrac{A_n}{V_n^+}, & \mathbf{r} \in T_n^+ \\ -\dfrac{A_n}{V_n^-}, & \mathbf{r} \in T_n^- \end{cases} \tag{27}$$

In order to ensure the normal continuity of $\mathbf{D}$ and $\mathbf{B}$, we express them as the linear combinations of the basis functions as:

$$\mathbf{D} = \frac{1}{j\omega}\sum_{n=1}^{N} D_n \mathbf{f}_n \tag{28}$$

$$\mathbf{B} = \frac{\eta_0}{j\omega}\sum_{n=1}^{N} B_n \mathbf{f}_n \tag{29}$$

and introduce the symmetric inner product:

$$\langle f, g\rangle = \int_V f \cdot g dV \tag{30}$$

thus, the equivalent volume current can be written as:

$$\mathbf{J}_V = \sum_{n=1}^{N} (D_n \bar{\boldsymbol{\beta}}_1 + B_n \eta_0 \bar{\boldsymbol{\beta}}_2) \cdot \mathbf{f}_n \tag{31}$$

$$\mathbf{M}_V = \sum_{n=1}^{N} (D_n \bar{\boldsymbol{\beta}}_3 + B_n \eta_0 \bar{\boldsymbol{\beta}}_4) \cdot \mathbf{f}_n \tag{32}$$

Applying Galerkin's procedure, volume integral equations can be converted into the linear equations:

$$\begin{bmatrix} \bar{\mathbf{Z}}^{ED} & \bar{\mathbf{Z}}^{EB} \\ \bar{\mathbf{Z}}^{HD} & \bar{\mathbf{Z}}^{HB} \end{bmatrix} \begin{bmatrix} D_n \\ B_n \end{bmatrix} = \begin{bmatrix} \mathbf{V}^E \\ \mathbf{V}^H \end{bmatrix} \tag{33}$$

where the elements of the block impedance matrices are:

$$
\begin{aligned}
Z_{mn}^{ED} &= \frac{1}{j\omega}\langle \mathbf{f}_m, \bar{\boldsymbol{\alpha}}_1 \cdot \mathbf{f}_n\rangle + j\omega\mu_0\langle \mathbf{f}_m, \mathbf{A}_{1,n}\rangle \\
&\quad -\frac{1}{j\omega\epsilon_0}\langle \mathbf{f}_m, \nabla\phi_{1,n}\rangle + \langle \mathbf{f}_m, \nabla\times\mathbf{A}_{3,n}\rangle
\end{aligned}
\tag{34}
$$

$$
\begin{aligned}
Z_{mn}^{EB} &= \eta_0\Big\{\frac{1}{j\omega}\langle \mathbf{f}_m, \bar{\boldsymbol{\alpha}}_2 \cdot \mathbf{f}_n\rangle + j\omega\mu_0\langle \mathbf{f}_m, \mathbf{A}_{2,n}\rangle \\
&\quad -\frac{1}{j\omega\epsilon_0}\langle \mathbf{f}_m, \nabla\phi_{2,n}\rangle + \langle \mathbf{f}_m, \nabla\times\mathbf{A}_{4,n}\rangle\Big\}
\end{aligned}
\tag{35}
$$

$$
\begin{aligned}
Z_{mn}^{HD} &= \eta_0\Big\{\frac{1}{j\omega}\langle \mathbf{f}_m, \bar{\boldsymbol{\alpha}}_3 \cdot \mathbf{f}_n\rangle + j\omega\epsilon_0\langle \mathbf{f}_m, \mathbf{A}_{3,n}\rangle \\
&\quad -\frac{1}{j\omega\mu_0}\langle \mathbf{f}_m, \nabla\phi_{3,n}\rangle - \langle \mathbf{f}_m, \nabla\times\mathbf{A}_{1,n}\rangle\Big\}
\end{aligned}
\tag{36}
$$

$$
\begin{aligned}
Z_{mn}^{HB} &= \eta_0^2\Big\{\frac{1}{j\omega}\langle \mathbf{f}_m, \bar{\boldsymbol{\alpha}}_4 \cdot \mathbf{f}_n\rangle + j\omega\epsilon_0\langle \mathbf{f}_m, \mathbf{A}_{4,n}\rangle \\
&\quad -\frac{1}{j\omega\mu_0}\langle \mathbf{f}_m, \nabla\phi_{4,n}\rangle - \langle \mathbf{f}_m, \nabla\times\mathbf{A}_{2,n}\rangle\Big\}
\end{aligned}
\tag{37}
$$

and the elements of the right hand side are:

$$
V_m^E = \langle \mathbf{f}_m, \mathbf{E}^{\mathrm{inc}}\rangle \tag{38}
$$

$$
V_m^H = \eta_0\langle \mathbf{f}_m, \mathbf{H}^{\mathrm{inc}}\rangle \tag{39}
$$

For the evaluation of the impedance matrix elements:

$$
\mathbf{A}_{i,n} = \int_{V_n} \bar{\boldsymbol{\beta}}_i \cdot \mathbf{f}_n G dV' = \frac{A_n}{3}\Big(\frac{\bar{\boldsymbol{\beta}}_{i,n}^{+}}{V_n^{+}} \cdot \int_{V_n^{+}} \rho_n^{+} G dV' \frac{\bar{\boldsymbol{\beta}}_{i,n}^{-}}{V_n^{-}} \cdot \int_{V_n^{-}} \rho_n^{-} G dV'\Big) \tag{40}
$$

$$
\begin{aligned}
\phi_{i,n} &= \int_{V_n} \nabla\cdot(\bar{\boldsymbol{\beta}}_i \cdot \mathbf{f}_n) G dV' = \frac{A_n}{3}\Big(\frac{\mathrm{Tr}(\bar{\boldsymbol{\beta}}_{i,n}^{+})}{V_n^{+}} \int_{V_n^{+}} G dV' - \frac{\mathrm{Tr}(\bar{\boldsymbol{\beta}}_{i,n}^{-})}{V_n^{-}} \int_{V_n^{-}} G dV' \\
&- \sum_{j=1}^{4} \hat{n}_{n,j}^{+} \cdot \frac{\bar{\boldsymbol{\beta}}_{i,n}^{+}}{V_n^{+}} \cdot \int_{\partial V_{n,j}^{+}} \rho_n^{+} G dS' - \sum_{j=1}^{4} \hat{n}_{n,j}^{-} \cdot \frac{\bar{\boldsymbol{\beta}}_{i,n}^{-}}{V_n^{-}} \cdot \int_{\partial V_{n,j}^{-}} \rho_n^{-} G dS'\Big)
\end{aligned}
\tag{41}
$$

$$
\begin{aligned}
&\langle \mathbf{f}_m, \nabla\times\mathbf{A}_{1,n}\rangle = \int_{V_m} \mathbf{f}_m \cdot \nabla\times\mathbf{A}_{1,n} dV \\
&= \int_{V_m} \mathbf{A}_{1,n} \cdot \nabla\times\mathbf{f}_m dV - \int_{V_m} \nabla\cdot(\mathbf{f}_m \times \mathbf{A}_{1,n}) dV \\
&= \frac{A_m}{3}\Big(-\sum_{j=1}^{4} \int_{\partial V_{m,j}^{+}} \hat{n}_{m,j}^{+} \cdot (\rho_m^{+} \times \mathbf{A}_{1,n}) dS
\end{aligned}
$$

$$-\sum_{j=1}^{4}\int_{\partial V_{m,j}^-}\hat{n}_{m,j}^-\cdot(\rho_m^-\times\mathbf{A}_{1,n})dS\Big) \tag{42}$$

where $\partial V_{m,j}^{\pm}$ denotes the $j$th face of the plus/minus tetrahedron associated with $m$th basis function, $\hat{n}_{m/n,j}^{\pm}$ denotes the outward normal vector of $j$th face of the plus/minus tetrahedron associated with $m/n$th basis function. $\mathrm{Tr}(\bar{\boldsymbol{\beta}})$ denotes the trace of the matrix $\bar{\boldsymbol{\beta}}$.

## 2.3. Adaptive Integral Method

The basic idea using AIM is to split the impedance matrix into two parts: near zone and far zone impedance matrix. Since the near zone impedance matrix is a sparse matrix, we can calculate the near zone interaction directly while use FFT to speed up the far zone interaction. Since FFT is being used, no need to store the whole far zone impedance matrix, which greatly reduce the memory requirement. Thus, the matrix vector multiplication can be written as:

$$\bar{\mathbf{Z}}\cdot\mathbf{I}=\bar{\mathbf{Z}}^{\mathrm{near}}\mathbf{I}+\bar{\mathbf{Z}}^{\mathrm{far}}\mathbf{I} \tag{43}$$

In employing AIM, the objects are first enclosed in a rectangular region and then recursively subdivided into small cells with each cell containing $(M+1)^3$ grids. Then each basis function will be projected to the surrounding grids of its associated cell. If we denote $\gamma_n$ as any component of $\left\{\mathbf{f}_n,\nabla\cdot\mathbf{f}_n,\bar{\boldsymbol{\beta}}_i\cdot\mathbf{f}_n,\nabla\cdot(\bar{\boldsymbol{\beta}}_i\cdot\mathbf{f}_n)\right\}$, the impedance matrix elements can be written in one uniform format:

$$Z_{mn}=\int_{V_m}\int_{V_n}\gamma_m G\gamma_n dV'dV \tag{44}$$

If $\gamma_m$ and $\gamma_n$ are far apart, the interaction between them can be approximated using delta functions. Under this situation, we can approximate $\gamma_n$ as the linear combination of delta functions:

$$\gamma_n(\mathbf{r})\approx\hat{\gamma}_n(\mathbf{r})=\sum_{u=1}^{(M+1)^3}\Lambda_{nu}\delta(\mathbf{r}-\mathbf{r}') \tag{45}$$

We can obtain $\Lambda_{nu}$ by matching the multiple moments of delta functions and original basis functions:

$$\int_{V_n}\gamma_n(\mathbf{r})(x-x_0)^{m1}(y-y_0)^{m2}(z-z_0)^{m3}dV$$
$$=\sum_{u=1}^{(M+1)^3}\Lambda_{nu}(x_{nu}-x_0)^{m1}(y_{nu}-y_0)^{m2}(z_{nu}-z_0)^{m3} \tag{46}$$

where $(x_0, y_0, z_0)$ is chosen as the center of the basis function. After obtaining coefficients $\Lambda_{nu}$, $Z_{mn}$ can be approximated as:

$$Z_{mn} \approx \hat{Z}_{mn} = \sum_{v=1}^{(M+1)^3} \sum_{u=1}^{(M+1)^3} \Lambda_{mv} G(\mathbf{r}_v, \mathbf{r}'_u) \Lambda_{nu} \tag{47}$$

written in matrix form:

$$\bar{\mathbf{Z}}^{\text{far}} = \bar{\mathbf{\Gamma}} \cdot \bar{\mathbf{G}} \cdot \bar{\mathbf{\Lambda}} \tag{48}$$

where $\bar{\mathbf{\Lambda}}$ is the projection matrix, $\bar{\mathbf{\Gamma}}$ is the interpolation matrix and $\bar{\mathbf{G}}$ is the Green's function matrix. Since $\bar{\mathbf{G}}$ is Toeplitz, we can use FFT to calculate the matrix vector multiplication. Thus,

$$\bar{\mathbf{Z}}^{\text{far}} \mathbf{I} = \bar{\mathbf{\Gamma}} \cdot \mathcal{F}^{-1} \left\{ \mathcal{F}\{\bar{\mathbf{G}}\} \cdot \mathcal{F}\{\bar{\mathbf{\Lambda}} \cdot \mathbf{I}\} \right\} \tag{49}$$

Since the near zone interaction can not be correctly approximated using the above method, we have to correct this interaction, thus we can define $\bar{\mathbf{Z}}^{\text{near}}$ as:

$$Z_{mn}^{\text{near}} = \begin{cases} Z_{mn} - \hat{Z}_{mn}, & d_{mn} \le d_{\text{near}} \\ 0, & \text{otherwise} \end{cases} \tag{50}$$

where $d_{\text{near}}$ is the near zone threshold distance. It is clear that $\bar{\mathbf{Z}}^{\text{near}}$ is a sparse matrix, thus matrix vector multiplication can be calculated directly. Therefore, the whole matrix vector multiplication can be written as:

$$\bar{\mathbf{Z}} \cdot \mathbf{I} = \bar{\mathbf{Z}}^{\text{near}} \mathbf{I} + \bar{\mathbf{\Gamma}} \cdot \mathcal{F}^{-1} \{ \mathcal{F}\{\bar{\mathbf{G}}\} \cdot \mathcal{F}\{\bar{\mathbf{\Lambda}} \cdot \mathbf{I}\}\} \tag{51}$$

In calculating the matrix elements, the curl operator is involved, then we use

$$\nabla \times \mathbf{F} = \left( \frac{\partial F_z}{\partial y} - \frac{\partial F_y}{\partial z} \right) \hat{x} + \left( \frac{\partial F_x}{\partial z} - \frac{\partial F_z}{\partial x} \right) \hat{y} + \left( \frac{\partial F_y}{\partial x} - \frac{\partial F_x}{\partial y} \right) \hat{z} \tag{52}$$

to calculate the derivative numerically through central difference scheme.

The matrix vector multiplication using AIM can be summarized as follow four steps:

(i) project $\bar{\boldsymbol{\beta}}_i \cdot \mathbf{f}_n$ and $\nabla \cdot (\bar{\boldsymbol{\beta}}_i \cdot \mathbf{f}_n)$ to surrounding grids;

(ii) calculate the grid potentials using FFT;

(iii) interpolate the grid potentials back to each basis function;

(iv) correct the near zone interaction.

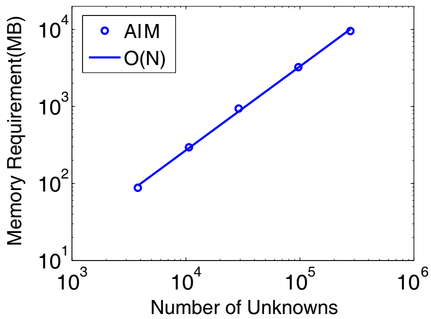


**Figure 1.** AIM memory requirement versus the number of unknowns.

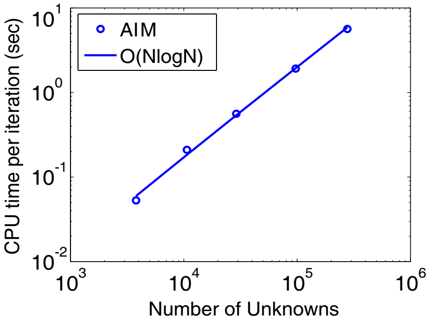


**Figure 2.** AIM CPU time per iteration versus the number of unknowns.

## 3. COMPUTATIONAL COMPLEXITY OF THE AIM

Now we investigate the computational complexity and storage requirement of our AIM implementation. We choose a spherical shell with inner radius 1m and the thickness 0.1 m as the example. It is composed of dielectric material with $\epsilon_r = 2$. The average length of the tetrahedral cell is $0.07\lambda_0$ where $\lambda_0$ is the free space wavelength. We increase the frequency of the incident plane wave gradually so that the total number of unknowns also increase. Then we record the the matrix storage requirement and CPU time per iteration, plotting them in Fig. 1 and Fig. 2, respectively. The asymptotic computational complexity and matrix storage requirement of AIM in solving volume integral equations have been given by [22] as of $O(N)$ and $O(N \log N)$, respectively. In our implementation on a PC, AIM exhibits $O(N)$, and $O(N \log N)$ patterns for the matrix storage and matrix vector multiplication, respectively. Our AIM implementation agrees well with the estimation given in [22].

## 4. NUMERICAL RESULTS

In this section, several examples will be given to demonstrate the validity and efficiency of our code to solve the electromagnetic scattering of large scale arbitrarily shaped bi-anisotropic objects. The GMRES solver is adopted as the iterative solver and it terminates when the normalized residue falls below $10^{-3}$. In the following examples, we will introduce some concepts such as bistatic RCS $\sigma$, co-polarized RCS

$\sigma_{\theta\theta}$ and cross-polarized RCS $\sigma_{\phi\theta}$ which are defined below:

$$\sigma = \lim_{r\to\infty} 4\pi r^2 \frac{|E^{\text{sca}}|^2}{|E^{\text{inc}}|^2} \tag{53}$$

$$\sigma_{\theta\theta} = \lim_{r\to\infty} 4\pi r^2 \frac{|E_\theta^{\text{sca}}|^2}{|E^{\text{inc}}|^2} \tag{54}$$

$$\sigma_{\phi\theta} = \lim_{r\to\infty} 4\pi r^2 \frac{|E_\phi^{\text{sca}}|^2}{|E^{\text{inc}}|^2} \tag{55}$$

where $E^{inc}$ is a $\theta$-polarized incident plane wave, $E_\theta^S$ and $E_\phi^S$ are respectively the $\theta$ and $\phi$ components of the scattered field produced.

### 4.1. Gyroelectric Spherical Shell

In the first example, we consider a gyroelectric spherical shell with inner radius $r_1 = 0.3\lambda_0$ and outer radius $r_2 = 0.6\lambda_0$ as an example to demonstrate the validity of our numerical solution. The constitutive parameters are: $\bar{\boldsymbol{\epsilon}} = \epsilon_0 \begin{pmatrix} 2.5 & j & 0 \\ -j & 2.5 & 0 \\ 0 & 0 & 1.5 \end{pmatrix}$. The structure of the spherical shell is shown in Fig. 3(a). The shell is discretized into 10,840 tetrahedron. The total number of unknowns is $N = 45,000$. The shell is illuminated by a plane wave with $k$ towards $z$ direction and $E$ in $x$

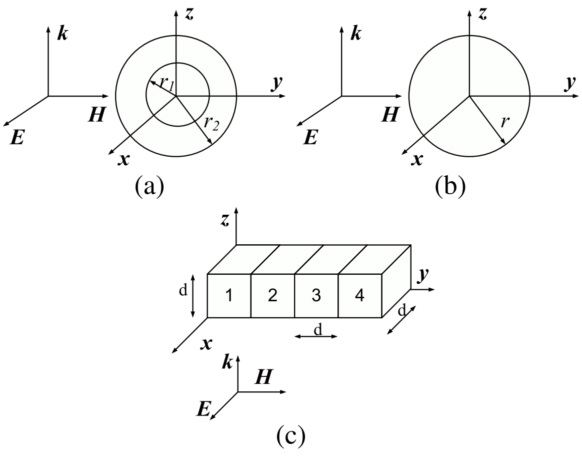


**Figure 3.** Geometries of bi-anisotropic objects considered as numerical examples. (a) A gyroeletric spherical shell, inner radius $r_1 = 0.3\lambda_0$, outer radius $r_2 = 0.6\lambda_0$. (b) A chiral sphere, radius $r = 0.8\lambda_0$. (c) A bi-anisotropic cubes, $d = \lambda_0$.

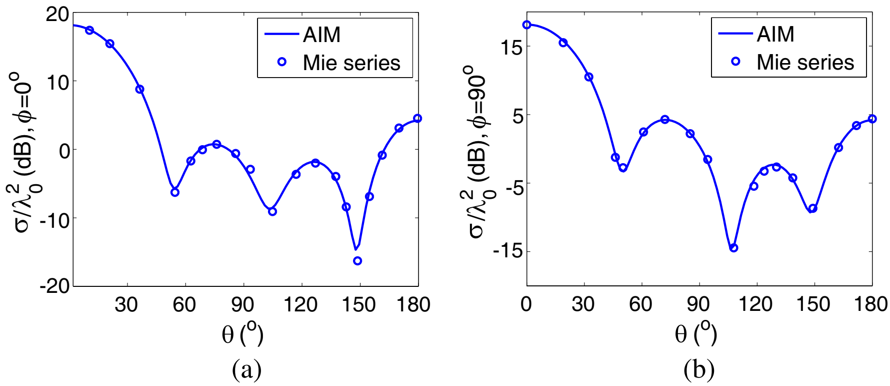


**Figure 4.** Total bistatic RCS of the shell in Fig. 3. (a) Total bistatic RCS for scattering angle $\phi = 0°$; (b) Total bistatic RCS for scattering angle $\phi = 90°$.

direction. Fig. 4 shows the bistatic RCS of the shell calculated using our code and also the Mie series [27] for comparison. We calculate the total Bistatic RCS in $x$-$z$ plane and $y$-$z$ plane respectively. From Fig. 4, we can conclude that the RCS results calculated from our code are in excellent agreement with Mie series. It is clear that the RCS results in two planes are similar, both have three valleys. However, the third valley is the deepest in $\phi = 0°$ plane, while it is the second valley that is the deepest in $\phi = 90°$ plane.

### 4.2. Chiral Sphere

In the second example, we consider a chiral sphere with radius $r = 0.8\lambda_0$ as an example to demonstrate the validity of our code. The constitutive parameters are: $\bar{\boldsymbol{\epsilon}} = 1.5\epsilon_0\bar{\mathbf{I}}$, $\bar{\boldsymbol{\mu}} = 1.5\mu_0\bar{\mathbf{I}}$, $\bar{\boldsymbol{\xi}} = -\bar{\boldsymbol{\zeta}} = -0.2j\sqrt{\epsilon_0\mu_0}\bar{\mathbf{I}}$. The structure of the sphere is shown in Fig. 3(b). The sphere is discretized into 27,256 tetrahedron. The total number of unknowns is $N = 111,294$. The shell is illuminated by a plane wave with $k$ towards $z$ direction and $E$ in $x$ direction. Fig. 5 shows the bistatic RCS of the sphere calculated using our code and also the Mie series [28] for comparison. From Fig. 5, we can conclude that the RCS results calculated from our code are in good agreement with Mie series. Some small discrepancy exists due to the inevitable numerical errors such as discretization errors and integration errors. We can see that there is a big difference between co-polarized and cross-polarized RCS. While there are many deep valleys for $\sigma_{\theta\theta}$, $\sigma_{\phi\theta}$ are much more smooth except when $\theta \approx 180°$ where both are very small.

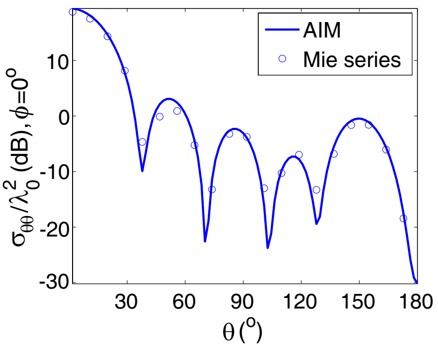


(a)

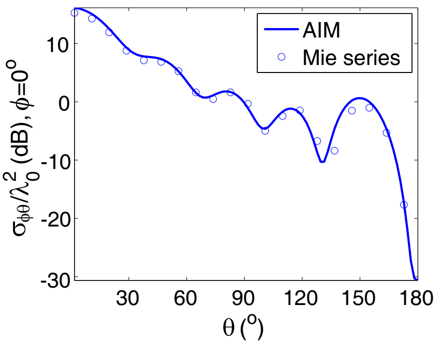


(b)

**Figure 5.** Bistatic RCS of the sphere in Fig. 3. (a) co-polarized Bistatic RCS for scattering angle $\phi = 0°$; (b) cross-polarized bistatic RCS for scattering angle $\phi = 0°$.

### 4.3. Bi-anisotropic Cubes

In the last example, we consider cubes with different constitutive parameters to demonstrate the versatility of our code in solving arbitrarily shaped large scale bi-anisotropic problems. There are four cubes along $y$ direction. The cubes' side lengths are $d = \lambda_0$. The first one is a gyroelectric cube with $\bar{\boldsymbol{\epsilon}} = \epsilon_0 \begin{pmatrix} 2.5 & j & 0 \\ -j & 2.5 & 0 \\ 0 & 0 & 1.5 \end{pmatrix}$. The second one is a gyromagnetic cube with $\bar{\boldsymbol{\mu}} = \mu_0 \begin{pmatrix} 2.5 & j & 0 \\ -j & 2.5 & 0 \\ 0 & 0 & 1.5 \end{pmatrix}$. The third one is a chiral cube with $\bar{\boldsymbol{\epsilon}} = 1.5\epsilon_0\bar{\mathbf{I}}$, $\bar{\boldsymbol{\mu}} = 1.5\mu_0\bar{\mathbf{I}}$, $\bar{\boldsymbol{\xi}} = -\bar{\boldsymbol{\zeta}} = -0.2j\sqrt{\epsilon_0\mu_0}\bar{\mathbf{I}}$. The last one is a Faraday chiral cube with $\bar{\boldsymbol{\epsilon}} = \begin{pmatrix} 2.5 & j & 0 \\ -j & 2.5 & 0 \\ 0 & 0 & 1.5 \end{pmatrix}$, $\bar{\boldsymbol{\mu}} = \begin{pmatrix} 2.5 & j & 0 \\ -j & 2.5 & 0 \\ 0 & 0 & 1.5 \end{pmatrix}$, $\bar{\boldsymbol{\xi}} = -\bar{\boldsymbol{\zeta}} = -0.2j\sqrt{\epsilon_0\mu_0}\bar{\mathbf{I}}$. The configuration of the cubes is shown in Fig. 3(c). The cubes are discretized into 54,129 tetrahedron. The total number of unknowns is $N = 221,880$. The cubes are illuminated by a plane wave with $k$ towards $z$ direction and $E$ in $x$ direction. Fig. 6 shows the bistatic RCS of the cubes. We have computed both co-polarized bistatic RCS for scattering angle $\phi = 0°$ and $\phi = 90°$, respectively. From these figures, we can see that for $\sigma_{\theta\theta}$, the result in $\phi = 0°$ plane is larger than that in $\phi = 90°$ plane except when $\theta > 120°$. For $\sigma_{\phi\theta}$, the result has many valleys in $\phi = 0°$ plane while only one deep valley in $\phi = 90°$ plane.

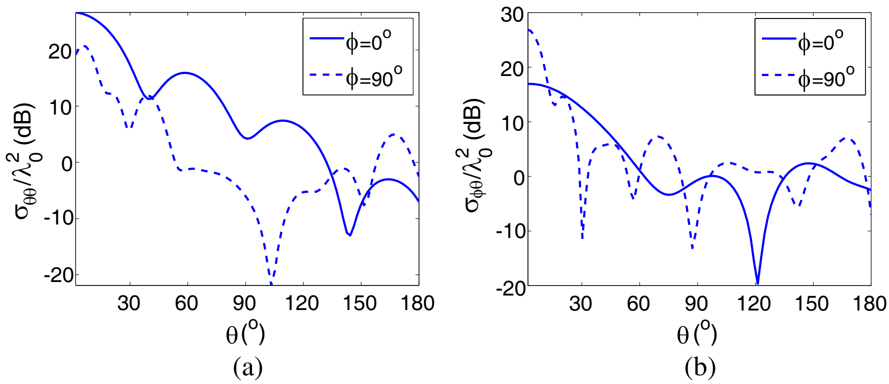


**Figure 6.** Bistatic RCS of the cubes in Fig. 3. (a) co-polarized bistatic RCS for scattering angle $\phi = 0^\circ$ and $\phi = 90^\circ$; (b) cross-polarized bistatic RCS for scattering angle $\phi = 0^\circ$ and $\phi = 90^\circ$.

**Table 1.** Comparison of memory requirement between AIM and MoM.

| Example | Unknowns | AIM (GB) | MoM (GB) | $M_{AIM}/M_{MoM}$ |
|---|---|---|---|---|
| shell | 45000 | 1.41 | 16.2 | 8.7% |
| sphere | 111294 | 3.78 | 99 | 3.8% |
| cube | 221880 | 7.56 | 394 | 1.9% |

**Table 2.** Comparison of CPU time between AIM and MoM.

| Example | Unknowns | AIM (hours) | MoM (hours) | $M_{AIM}/M_{MoM}$ |
|---|---|---|---|---|
| shell | 45000 | 1.0 | 5.4 | 19% |
| sphere | 111294 | 2.2 | 82 | 2.7% |
| cube | 221880 | 4.4 | 646 | 0.7% |

## 4.4. Memory and CPU Time Comparison

In Table 1, we compare the total memory consumed by AIM and the memory estimated for the conventional MoM in computing these examples. From Table 1, we observe that the memory savings using AIM is more than 90%.

The CPU time consumed by AIM to compute these examples is shown in Table 2 and CPU time estimated for MoM is also given for comparison purpose. We find that the saving in time is more than 80%.

## 5. CONCLUSION

In this paper, adaptive integral method has been extended to solve the electromagnetic scattering by large scale inhomogeneous bi-anisotropic objects. Volume integral equations are used to characterize the scattering property of bi-anisotropic objects and subsequently converted into a matrix equation by using MoM. AIM has been utilized to reduce the stringent memory requirement and to speed up the solution process. The gyroelectric spherical shell and chiral sphere examples are used to validate our AIM code and the bi-anisotropic cubes example is used to demonstrate the versatility of AIM code in solving scattering problems by large scale arbitrarily shaped objects.

## REFERENCES

1. Serdyukov, A., I. Semchenko, S. Tretyakov, and A. Sihvola, *Electromagnetics of Bi-anisotropic Materials: Theory and Applications*, Taylor & Francis, 2001.
2. Qiu, C. W., H. Y. Yao, L. W. Li, S. Zouhdi, and T. S. Yeo, "Backward waves in magnetoelectrically chiral media: Propagation, impedance and negative refraction," *Phys. Rev. B*, Vol. 75, 155120, Apr. 2007.
3. Qiu, C. W., H. Y. Yao, S. Zouhdi, L. W. Li, and M. S. Leong, "On the constitutive relations of G-chiral media and the possibility to realize negative-index media," *Microwave Opt. Technol. Lett.*, Vol. 48, No. 12, 2534–2538, Dec. 2006.
4. Shen, J., "Negative refractive index in gyrotropically magneto-electric media," *Phys. Rev. B*, Vol. 73, 045113, Jan. 2006.
5. Qiu, C. W. and S. Zouhdi, "Comment on 'Negative refractive index in gyrotropically magnetoelectric media'," *Phys. Rev. B*, Vol. 19, 196101, May 2007.
6. Dong, W., L. Gao, and C. W. Qiu, "Goos-Hänchen shift at the surface of chiral negative refractive media," *Progress In Electromagnetics Research*, PIER 90, 255–268, 2009.
7. Viitanen, A. J. and I. V. Lindell, "Chiral slab polarization transformer for aperture antennas," *IEEE Trans. Antennas Propagat.*, Vol. 46, 1395–1397, Sept. 1998.
8. Chiu, C. N. and C. G. Hsu, "Scattering and shielding properties of a chiral-coated fiber-reinforced plastic composite cylinder," *IEEE Trans. Electromagn. Compat.*, Vol. 47, 123–130, Feb. 2005.
9. Gao, L., T. H. Fung, K. W. Yu, and C. W. Qiu, "Electromagnetic

transparency by coated spheres with radial anisotropy," *Phys. Rev. E*, Vol. 78, 046609, Oct. 2008.
10. Lukyanchuk, B. and C. W. Qiu, "Enhanced scattering efficiencies in spherical particles with weakly dissipating anisotropic materials," *Appl. Phys. A*, Vol. 92, 773–776, May 2008.
11. Qiu, C. W., S. Zouhdi, and A. Razek, "Modified spherical wave functions with anisotropy ratio: Application to the analysis of scattering by multilayered anisotropic shells," *IEEE Trans. Antennas Propagat.*, Vol. 55, No. 12, 3515–3523, Dec. 2007.
12. Hanson, G. W., "A numerical formulation of dyadic greens functions for planar bianisotropic media with application to printed transmission lines," *IEEE Trans. Microwave Theory Tech.*, Vol. 44, No. 1, 144–151, Jan. 1996.
13. Bohren, C. F. and D. R. Huffman, *Absorption and Scattering of Light by Small Particles*, Wiley, 1983.
14. Tarento, R.-J., K.-H. Bennemann, P. Joyes, and J. Van de Walle, "Mie scattering of magnetic spheres," *Phys. Rev. E*, Vol. 69, No. 2, 026606, 2004.
15. Geng, Y.-L., X.-B. Wu, L.-W. Li, and B.-R. Guan, "Mie scattering by a uniaxial anisotropic sphere," *Phys. Rev. E*, Vol. 70, No. 5, 056609, Nov. 2004.
16. Demir, V., A. Z. Elsherbeni, and E. Arvas, "FDTD formulation for dispersive chiral media using the Z transform method," *IEEE Trans. Antennas Propagat.*, Vol. 53, 3374–3384, Oct. 2005.
17. Valor, L. and J. Zapata, "An efficient finite element formulation to analyze waveguides with lossy inhomogeneous bi-anisotropic materials," *IEEE Trans. Microwave Theory Tech.*, Vol. 44, 291–296, Feb. 1996.
18. Bilotti, F., A. Toscano, and L. Vegni, "Fem-bem formulation for the analysis of cavity-backed patch antennas on chiral substrates," *IEEE Trans. Antennas Propagat.*, Vol. 51, 306–311, Feb. 2003.
19. Schaubert, D. H., D. R. Wilton, and A. W. Gilsson, "A tetrahedral modeling method for electromagnetic scattering by arbitrarily shaped inhomogeneous dielectric bodies," *IEEE Trans. Antennas Propagat.*, Vol. 32, No. 1, 77–85, Jan. 1984.
20. Su, C. C., "Electromagnetic scattering by a dielectric body with arbitrary inhomogeneity and anisotropy," *IEEE Trans. Antennas Propagat.*, Vol. 37, 384–389, Mar. 1989.
21. Hasanovic, M., C. Mei, J. Mautz, and E. Arvas, "Scattering from 3-D inhomogeneous chiral bodies of arbitrary shape by the Method of Moments," *IEEE Trans. Antennas Propagat.*, Vol. 55, 1817–

1825, Jun. 2007.

22. Bleszynski, E., M. Bleszynski, and T. Jaroszewicz, "AIM: Adaptive integral method for solving large-scale electromagnetic scattering and radiation problems," *Radio Sci.*, Vol. 31, No. 5, 1225–1252, 1996.
23. Nie, X.-C., N. Yuan, and L.-W. Li, "Precorrected-FFT algorithm for solving combined field integral equations in electromagnetic scattering," *Journal of Electromagnetic Waves and Applications*, Vol. 16, No. 8, 1171–1187, 2002.
24. Ewe, W. B., L. W. Li, and M. S. Leong, "Solving mixed dielectric/conducting scattering problem using adaptive integral method," *Progress In Electromagnetics Research*, PIER 46, 143–163, 2004.
25. Nie, X. C., N. Yuan, L. W. Li, T. S. Yeo, and Y. B. Gan, "Fast analysis of electromagnetic transmission through arbitrarily shaped airborne radomes using precorrected-fft method," *Progress In Electromagnetics Research*, PIER 54, 37–59, 2005.
26. Ewe, W. B., E. P. Li, H. S. Chu, and L. W. Li, "AIM analysis of electromagnetic scattering by arbitrarily shaped magnetodielectric object," *IEEE Trans. Antennas Propagat.*, Vol. 55, No. 7, 2073–2079, Jul. 2007.
27. Geng, Y.-L., X.-B. Wu, and L.-W. Li, "Characterization of electromagnetic scattering by a plasma anisotropic spherical shell," *IEEE Antennas and Wireless Propagat. Lett.*, Vol. 3, 100–103, 2004.
28. Bohren, C. F., "Light scattering by an optically active sphere," *Chem. Phys. Lett.*, Vol. 29, 458–462, 1974.